Molecular Neurobiology (2019) 56:3420–3436
https://doi.org/10.1007/s12035-018-1293-4

The Prion Protein Regulates Synaptic Transmission by Controlling the Expression of Proteins Key to Synaptic Vesicle Recycling and Exocytosis

Caterina Peggion[1] · Roberto Stella[2] · Francesco Chemello[3] · Maria Lina Massimino[4] · Giorgio Arrigoni[1,5] · Stefano Cagnin[3] · Giancarlo Biancotto[2] · Cinzia Franchin[1,5] · Maria Catia Sorgato[1,4] · Alessandro Bertoli[1,6]

Received: 10 May 2018 / Accepted: 1 August 2018 / Published online: 20 August 2018
© Springer Science+Business Media, LLC, part of Springer Nature 2018

Abstract

The cellular prion protein (PrP^C), whose misfolded conformers are implicated in prion diseases, localizes to both the presynaptic membrane and postsynaptic density. To explore possible molecular contributions of PrP^C to synaptic transmission, we utilized a mass spectrometry approach to quantify the release of glutamate from primary cerebellar granule neurons (CGN) expressing, or deprived of (PrP-KO), PrP^C, following a depolarizing stimulus. Under the same conditions, we also tracked recycling of synaptic vesicles (SVs) in the two neuronal populations. We found that in PrP-KO CGN these processes decreased by 40 and 60%, respectively, compared to PrP^C-expressing neurons. Unbiased quantitative mass spectrometry was then employed to compare the whole proteome of CGN with the two PrP genotypes. This approach allowed us to assess that, relative to the PrP^C-expressing counterpart, the absence of PrP^C modified the protein expression profile, including diminution of some components of SV recycling and fusion machinery. Subsequent quantitative RT-PCR closely reproduced proteomic data, indicating that PrP^C is committed to ensuring optimal synaptic transmission by regulating genes involved in SV dynamics and neurotransmitter release. These novel molecular and cellular aspects of PrP^C add insight into the underlying mechanisms for synaptic dysfunctions occurring in neurodegenerative disorders in which a compromised PrP^C is likely to intervene.

Keywords Prion protein · Neurotransmission · Synaptic vesicle · Mass spectrometry · Selected reaction monitoring · Gene expression

Introduction

The cellular prion protein (PrP^C) is a glycoprotein highly conserved in the vertebrate sub-phylum. It is abundantly expressed in lymphoreticular organs and in all brain areas. It anchors to the external cell surface through a glycolipid moiety and in neurons it clusters preferentially along axons and in both the presynaptic terminal [1, 2] and postsynaptic density [3, 4].

It is well established that PrP^C aberrant misfolding generates PrP^{Sc}, the principal component of prions causing

Caterina Peggion and Roberto Stella contributed equally to this work.

Electronic supplementary material The online version of this article (https://doi.org/10.1007/s12035-018-1293-4) contains supplementary material, which is available to authorized users.

✉ Caterina Peggion
catpeg@outlook.it

✉ Alessandro Bertoli
alessandro.bertoli@unipd.it

[1] Department of Biomedical Sciences, University of Padova, 35131 Padova, Italy

[2] Department of Chemistry, Istituto Zooprofilattico Sperimentale delle Venezie, 35020 Legnaro, PD, Italy

[3] Department of Biology, University of Padova, 35131 Padova, Italy

[4] CNR—Neuroscience Institute, University of Padova, 35131 Padova, Italy

[5] Proteomics Center, University of Padova and Azienda Ospedaliera di Padova, 35129 Padova, Italy

[6] Padova Neuroscience Center, University of Padova, 35131 Padova, Italy

transmissible prion disorders (or spongiform encephalopathies), including Creutzfeldt–Jacob disease in human, scrapie in sheep, and bovine spongiform encephalopathy in cattle [5]. Spreading of the disease is ensured by the capacity of PrP^{Sc} to act as template for further PrP^{C}-to-PrP^{Sc} conformational conversion [6], which explains why PrP^{C}-deprived (PrP-KO) models are resistant to prion diseases and do not propagate prions [7, 8].

Intriguingly, however, PrP^{C} function in the central nervous system is yet to be definitively recognized. Major conceptual obstacles to the full understanding of PrP^{C} physiology are the lack of obvious phenotypes in PrP-KO mice [9, 10], and the extensive pleiotropicity of PrP^{C}—in terms of both interacting partners and advantageous functions to the cell life—as it resulted from year-long comparison of PrP^{C}-expressing paradigms with PrP-KO, or PrP-mutant, counterparts [11–15, for recent reviews]. Notably, PrP^{C} multi-faceted aspect could be now revisited under novel frameworks. For example, the dichotomic structure of PrP^{C}—only the C-terminus has stable secondary and tertiary folding [16]—assigns the protein to the "intrinsically disordered protein" family [17, 18] and, accordingly, to serving as central hub in the coordination and integration of multiple signaling networks. A complementary framework envisages that PrP^{C} acts as a cell surface scaffold protein that organizes diverse signaling modules in a cell- and context-dependent manner [12]. In both views, the interaction of PrP^{C} with a variety of proteins would allow transduction of beneficial signals to cells, and to neurons in particular.

Intuitively, the large spectrum of PrP^{C} interactors may well include neurotoxic species that, by preferentially binding the intrinsically disordered N-terminus of PrP^{C} [19, 20], may provoke synaptic and cognitive deficits. This assumption has been proven correct for prions (in a process however distinct from PrP^{C}-to-PrP^{Sc} conversion [20]), Alzheimer's disease-related soluble Aβ oligomers, and, more recently, α-synuclein prefibrillar oligomers [21], or fibrils [22, 23], which are associated to synucleinopathies such as Parkinson's disease. Undoubtedly, these findings enrich PrP^{C} pathophysiological traits, yet they are unable to fully unveil the mechanisms linking PrP^{C} to synaptic damage. A sensible hypothesis, however, would entail that the binding of oligomers to PrP^{C} compromises the beneficial attributes of the protein, such as the safeguard of synaptic transmission, and/or of synaptic plasticity and its correlate long-term potentiation involved in learning and memory [24–30].

To deepen the role of PrP^{C} in synapses, and to reveal possible consequences of PrP^{C} dysregulation, here we have compared the outcome of depolarization-induced fusion of synaptic vesicles (SVs) with the presynaptic plasma membrane in PrP^{C}-expressing, and PrP-KO, primary cerebellar granule neurons (CGN). This analysis demonstrated that PrP-KO neurons have defective neurotransmitter secretion and compromised exo-endocytotic cycle of SVs, compared to PrP^{C}-expressing counterparts. Protein expression profiles of the two cell populations, obtained by quantitative mass spectrometry (MS)-based approach and selected reaction monitoring (SRM), showed that deprivation of PrP^{C} led to reduced amounts of some proteins implicated in the above processes. Quantification of their corresponding mRNAs confirmed the proteomic results, while bioinformatic approaches and biochemical data suggested that the transcription factor cAMP response element-binding protein 1 (Creb1) was the likely key intermediate in the PrP^{C}-gene transcription axis. The present study is therefore strongly suggestive that the underlying mechanism enabling PrP^{C} to grant efficient neurotransmitter secretion is the modulation of genes coding for proteins regulating SV physiology.

Materials and Methods

Animal Care and Use

We used PrP-KO mice (line F10) and, as control, transgenic (PrP-Tg) mice (line Tg46) in which the expression of PrP^{C} at normal levels was rescued over the PrP-KO genotype [31]. Both co-isogenic strains were kindly provided by the M.R.C. Prion Unit, London, UK. Animals were housed in a temperature-controlled (22 °C) room with a 12:12 h light:dark cycle, with ad libitum access to food and water. All aspects of animal care and experimentation were performed in compliance with European and Italian (D.L. 26/2014) laws concerning the care and use of laboratory animals. All experimental procedures and animal care protocols were approved by the Italian Ministry of Health (authorization n. 743/2017-PR) and by the Ethical Committee for animal care and use of the University of Padova. All efforts were made to minimize animal suffering and reduce the number of animals used in the experiments.

Cerebellar Granule Neuron Culturing

To obtain primary cultures, cerebellar granule neurons (CGN) were isolated from 7 day-old mice (decapitated after anesthesia with methoxyflurane) as previously described [32]. Neurons were grown in minimal essential medium supplemented with 10% heat-inactivated fetal calf serum, 2 mM L-glutamine, 0.1 mg/ml gentamycin, and KCl (25.4 mM K^{+} final concentration), seeded onto poly-L-lysine (100 μg/ml; Sigma-Aldrich, cat. no. P636)-coated 35 mm-diameter wells at a density of 350,000 cells/cm^2, and maintained at 37 °C in a humidified incubator with a 5% CO_2 atmosphere. To prevent proliferation of mitotic (non-neuronal) cells, cytosine-1-β-D-arabinofuranoside (10 μM; Sigma-Aldrich) was added to cells 24 h after plating. In all experiments, CGN were used after 96 h of culturing.

Quantification of Glutamate Release by LC-MS

The release of glutamate by CGN was measured under depolarizing conditions. Briefly, after rinsing twice with Krebs Ringer buffer solution (KRB, NaCl 125 mM, KCl 5 mM, $CaCl_2$ 1 mM, KH_2PO_4 0.5 mM, $MgSO_4$ 1 mM, glucose 5.5 mM, HEPES 20 mM, pH 7.4), cells were incubated (5 min) in 500 μl of KRB containing 60 mM KCl, after which the medium was collected, centrifuged (10 min, 16,000×*g*, 4 °C) to remove cell debris, and acidified (pH < 3) with formic acid (FA; Sigma-Aldrich). The medium was subsequently diluted (1:1, *v*/*v*) with acetonitrile prior to liquid chromatography (LC)-MS analysis. Cells incubated in KRB with no added KCl were used as negative control. To verify the effective implication of SVs in glutamate release, another control consisted in adding to CGN (30 min, prior to the depolarizing step) botulinum toxin (BoNT/D, 10 nM; a kind gift of Dr. C. Montecucco, University of Padova, Italy), which inhibits SV exocytosis.

The LC-MS system used for glutamate quantification was a Thermo Ultimate 3000 UHPLC coupled to a Q-Exactive (quadrupole-Orbitrap) mass spectrometer (Thermo Fisher Scientific). The UHPLC system was equipped with a Zic-HILIC column (100 × 2.1 mm, 3.5 μm particle size; Merck) kept at 35 °C. Elution solvents were water (a) and acetonitrile (b), both containing FA 0.1% (*v*/*v*). The mobile phase composition (a:b) was 5:95 from 0 to 0.5 min; changed linearly from 5:95 to 60:40 between 0.5 and 5 min; 60:40 from 5 to 7.25 min; changed linearly from 60:40 to 5:95 between 7.25 and 7.5 min; 5:95 from 7.5 to 10.0 min. The injection volume was 5 μl and the flow rate was 0.350 ml/min.

High-resolution MS signals were acquired using targeted SIM scan mode, recording the ion with the *m*/*z* value expected for glutamic acid (148.0604), and applying an isolation window of 2.0 *m*/*z* (with a resolving power of 70,000 full width at half maximum, at 200 *m*/*z*). Source parameters were as follows: spray voltage, 3.5 kV in positive polarity; capillary temperature, 325 °C; sheath gas flow rate, 35 arbitrary units; auxiliary gas flow rate, 10 arbitrary units; S-lens voltage, 50 V; in-source fragmentation voltage, 0; heater temperature, 325 °C. To quantify glutamate in samples, MS raw data were processed using the software Quant Browser (Thermo Fisher Scientific) by extracting the *m*/*z* at 148.0604 with a tolerance of 5 ppm, thanks to a six-point glutamate calibration curve (0.25, 1.00, 1.75, 2.50, 3.25, 4.00 μM).

Measured glutamate concentrations were then normalized to the total protein content of the corresponding CGN sample. To this purpose, neurons were washed twice with ice-cold phosphate-buffered saline (PBS) and lysed in an ice-cold lysis buffer [glycerol 10% (*w*/*v*), sodium dodecyl-sulfate (SDS) 2% (*w*/*v*), Tris/HCl 62.5 mM, pH 6.8, Na_3VO_4 5 mM, and cocktails of protease and phosphatase inhibitors (Roche)]. Lysates were centrifuged (10 min, 14,000×*g*, 4 °C) to remove cell debris, while, here and after, protein concentration was determined with a Lowry assay kit (Sigma-Aldrich).

Assay for SV Recycling

Experiments were performed according to Ref. [33]. Briefly, CGN were washed twice with KRB, kept (10 min) in the same buffer added with KCl (60 mM final concentration; depolarizing conditions) promoting SV recycling (i.e., fusion to the plasma membrane followed by endocytosis), and further incubated (20 min) in the presence, or in the absence, of a mouse monoclonal antibody (5 μg/ml) to synaptotagmin 1 (Syt1; Synaptic Systems, cat. no. 105011). When indicated, neurons were pre-incubated (30 min) in KRB with BoNT/D (10 nM). CGN were then lysed (using the above lysis buffer under non-reducing conditions) and the protein content determined as described above. Lysates were adjusted to an equal protein concentration utilizing a non-reducing sample buffer [glycerol 10% (*w*/*v*), SDS 2% (*w*/*v*), Tris/HCl 62.5 mM, pH 6.8, bromophenol blue 0.02% (*w*/*v*)], and then subjected to SDS-PAGE and Western blot (see below), using a horseradish peroxidase-conjugated antibody raised against mouse IgGs (Santa Cruz Biotechnology, cat. no. sc-2005) to detect the SV-internalized anti-Syt1 antibody.

Cell Lysis and Protein Extraction

For proteomic and Western blot analyses, neurons were washed twice with ice-cold PBS, lysed in the above ice-cold lysis buffer (80 μl), and centrifuged as above to remove cell debris. Protein-containing supernatants were then stored at − 80 °C until use. When needed, samples were brought to an equal protein concentration using the above sample buffer under reducing conditions (i.e., added with dithiothreitol, 50 mM final concentration; Sigma-Aldrich) and boiled (5 min).

Protein Digestion and Stable Isotope Dimethyl Labeling

Protein samples (30 μg) were loaded onto SDS-polyacrylamide [5% (*w*/*v*); acrylamide/bisacrylamide, 37.5:1] gels, and the electrophoretic process was allowed to proceed until proteins converged to a tight band. Bromophenol blue-stained bands were manually cut in small slices, washed twice in H_2O, dehydrated with acetonitrile (400 μl, 10 min), and dried under vacuum. Reduction of disulfide bonds was accomplished by rehydrating gel slices in 300 μl of 50 mM triethylammonium bicarbonate (Sigma-Aldrich, cat. no. T7408) containing 10 mM dithiothreitol. After 1 h at 56 °C, the dithiothreitol-containing solution was substituted with an equal volume of triethylammonium bicarbonate (50 mM) containing 55 mM iodoacetamide (Sigma-

Aldrich, cat. no. E006125) to alkylate the reduced cysteine residues. Samples were incubated in the dark (45 min, RT), washed four times (300 μl, 10 min each) by alternating triethylammonium bicarbonate (25 mM) and acetonitrile, and finally dried under vacuum.

Proteins were digested by reconstituting gel samples in 90 μl of a sequencing grade-modified trypsin solution (12.5 ng/ml in 50 mM triethylammonium bicarbonate; Promega, cat. no. V5117) and incubating them overnight at 37 °C. Then, peptides were extracted by incubating gel slices (10 min, RT) in 300 μl of acetonitrile 50% (*v*/*v*) and FA 0.1% (*v*/*v*). This procedure was repeated three times, and the total peptide extract solution (900 μl) was collected and dried under vacuum. Subsequently, an on-column isotopomeric dimethylation procedure was carried out to chemically label peptides [34]. To this purpose, peptide samples from the three biological replicates of PrP-Tg and PrP-KO CGN were resuspended in 1 ml of FA 5% (*v*/*v*) and loaded onto acetic acid [0.6% (*v*/*v*)]-preconditioned C18 cartridges (SepPak Vac 1cc; Waters, cat. no. WAT023590). Subsequently, peptides were labeled by flushing cartridges with 5 ml of a cyanoborohydride (Sigma-Aldrich, cat. no. 156159, 30 mM in a sodium/phosphate buffer)-based reagent containing either a "light" [formaldehyde-H_2 0.2% (*v*/*v*); Sigma-Aldrich, cat. no. 15513-M] or a "heavy" [formaldehyde-D_2 0.2% (*v*/*v*); Sigma-Aldrich, cat. no. 492620] molecular tag. Columns were then rinsed twice with acetic acid [0.6% (*v*/*v*)] and peptides were eluted using a solution containing acetonitrile 80% (*v*/*v*) and acetic acid 0.6% (*v*/*v*), vacuum-dried, and resuspended in 30 μl of a solution with acetonitrile 3% (*v*/*v*) and FA 0.1% (*v*/*v*). Finally, (light/heavy) PrP-Tg-derived and (heavy/light) PrP-KO-derived labeled peptides were mixed together, in a 1 : 1 ratio (PrP-Tg/PrP-KO), to generate three replicates (60 μl each) of combined PrP-Tg/PrP-KO samples (Supplementary Fig. S1).

Sample Fractionation by Strong Cation Exchange

To reduce sample complexity, the three PrP-Tg/PrP-KO combined samples were subjected to fractionation by strong cation exchange. Firstly, samples were 15-fold diluted in an equilibration buffer (5 mM KH_2PO_4, 25% acetonitrile, pH 3) and loaded (at a 50 μl/min flow rate) onto strong cation-exchange cartridges (AB Sciex, cat. no. 4326695). After thoroughly washing cartridges with the equilibration buffer, retained peptides were then stepwise eluted in five fractions by increasing KCl concentration, using the above buffer (900 μl) added with 50, 100, 150, 200, or 350 mM KCl (final concentration). Fractions were vacuum-dried, resuspended in 1 ml of FA 0.1% (*v*/*v*), desalted using SepPak Vac C18 cartridges, according to manufacturer's instructions, vacuum-dried, and finally dissolved in 50 μl of a solution of acetonitrile 3% (*v*/*v*), and FA 0.1% (*v*/*v*), just prior to LC-MS/MS analysis.

LC-MS/MS Analysis

Analysis of CGN proteomes was performed using a LTQ-Orbitrap XL mass spectrometer (Thermo Fisher Scientific) coupled with an on-line nano-HPLC Ultimate 3000 (Dionex; Thermo Fisher Scientific).

Each of the fractions (3 μg) originating from the strong cation-exchange step was loaded onto a Trap column [300 μm internal diameter, 300 Å, C18, 3 μm (SGE Analytical Science, cat. no. 2227054)] by the integrated auto-sampler using FA 0.1% (*v*/*v*) (8 μl/min flow rate), and transferred into a 10 cm Picofrit® column [75 μm internal diameter, 15 μm tip (New Objective, cat. no. PF751510XXXX)] packed with C18 material (Aeris Peptide 3.6 μm XB-C18; Phenomenex). The liquid chromatographic separation of peptides was carried out, at a flow rate of 250 nl/min, using water (a) and acetonitrile (b) [both containing FA 0.1% (*v*/*v*)] as elution solvents in the following composition (expressed as a:b ratio): 97:3 for 6 min; from 97:3 to 50:50 in 90 min (following a linear gradient), from 50:50 to 20:80 in 2 min; 20:80 for 5 min; back to 97:3 (to re-equilibrate the system).

The temperature of the ion source capillary was set at 200 °C, the spray was optimized at 1.3 kV, and the mass spectrometer operated in data-dependent mode with a top-4 acquisition method (i.e., a full scan at a 60,000 resolution on the Orbitrap, followed by the MS/MS fragmentation in the linear trap of the four most intense ions). To increase the number of identified peptides and proteins, each fraction of the strong cation exchange procedure was analyzed twice. To this purpose, the *m*/*z* values of peptides positively identified in the first analysis (as described in detail in the next section) were used to create a static exclusion list that was then applied to a second LC-MS/MS analysis (under the same chromatographic and instrumental conditions) for each sample fraction.

Untargeted MS Data Analysis

Raw files derived from LC-MS/MS runs were analyzed with a MudPIT protocol using the Proteome Discoverer 1.4 software (Thermo Fisher Scientific) interfaced to a Mascot search engine (version 2.2.4; Matrix Science). All MS/MS data were searched against the UniProt *Mus musculus* database (version 20150401; 53,301 sequences). Enzyme specificity was set to trypsin, and a maximum of two missed cleavages were allowed. The precursor and product ion mass tolerances were set to 10 ppm and 0.6 Da, respectively. While modifications of N-terminal and lysine residues [light-label dimethylation (+28.0313 Da); heavy-label dimethylation (+32.0564 Da)] were set as variable, carbamidomethylation of cysteines was set as fixed.

Quantification was performed directly by the Proteome Discoverer software and only unique peptides were

considered for quantification purposes. Based on the Percolator algorithm, proteins were considered as correctly identified if at least two unique peptides were quantified with an individual q value < 0.01 (99% confidence) and rank 1. Proteins were then grouped according to the principle of maximum parsimony. Only protein groups that were identified and quantified in all six biological replicates were considered for further analysis. Quantification was performed by normalizing each (PrP-KO/PrP-Tg) ratio obtained in a given replicate to the median value of all measured ratios in that replicate. The final fold change of a given protein was calculated as the mean value of the normalized ratios of the three replicates. Finally, a two-tailed Z test was performed, and only proteins with a ratio PrP-KO/PrP-Tg > 1.3 or < 0.77, and a p value < 0.05, were considered as overexpressed or underexpressed, respectively.

Selected Reaction Monitoring Confirmation Study

For selected reaction monitoring (SRM) experiments, CGN lysates from six CGN cultures for each PrP genotype were obtained using the above lysis buffer, and proteins were quantified as described. Protein extracts (50 μg, 50 μl) from each lysate were processed according to the filter-aided sample preparation method [35], using filters with 10,000 Da as molecular weight cut-off (Sartorius, cat. no. VN01H02) and the FASP™ protein digestion kit (Expedeon, cat. no. 44250) following manufacturer's instructions. During sample processing, cysteine residues were reduced and alkylated using 20 mM dithiothreitol (45 min, 56 °C) and 55 mM iodoacetamide (45 min in the dark, RT), respectively. Subsequently, sequencing grade-modified trypsin (Promega) was added (90 μl in 25 mM NH_4HCO_3) to a final enzyme/protein ratio of 1:25 (*w*/*w*), and protein digestion was carried out overnight (37 °C). Finally, filter units were centrifuged (14,000×*g*, 10 min) to recover peptides. To improve recovery, filters were rinsed with 50 μl of 25 mM NH_4HCO_3 and centrifuged again. Peptide solutions were acidified (pH < 3) by adding FA, and desalted using C18 spin columns (The Nest Group, cat. no. SMM-SS18V), following manufacturer's instructions, with the exception that two sequential elution steps—with a solution (100 μl) containing acetonitrile 70% (*v*/*v*) and FA 0.1% (*v*/*v*)—were performed. Finally, peptide extracts were dried under vacuum and, immediately before LC-MS/MS analyses, dissolved in a solution (100 μl) containing acetonitrile 5% (*v*/*v*) and FA 0.1% (*v*/*v*) to obtain a final concentration of 0.5 $\mu g \times \mu l^{-1}$ of protein digest.

Analysis was performed using a Prominence HPLC system (Shimadzu) interfaced to an API 4000 triple quadrupole mass spectrometer (AB Sciex), operating in SRM mode with a scheduled method. The mass spectrometer source parameters were as follows: 5000 V as ion spray voltage; 500 °C as source temperature; 15 psi for curtain gas; 35 psi for both Gs1 and Gs2.

The liquid chromatographic separation was achieved using a Brownlee SPP peptide ES-C18 column (100 × 2.1 mm, 2.7 μm; Perkin Elmer, cat. no. N9308453), injecting 10 μl of sample for each analysis. Peptide separation was carried out (at a flow rate of 0.3 ml/min) using water (a) and acetonitrile (b) [both containing FA 0.1% (*v*/*v*)] as elution solvents in the following composition (expressed as a:b ratio): 95:5 for 1 min; from 95:5 to 65:35 in 14 min (following a linear gradient); from 65:35 to 45:55 in 2.5 min; from 45:55 to 5:95 in 1 min; kept unchanged for 2 min; and finally set to 97.5:2.5 from 21 to 25 min to re-equilibrate the system.

The scheduled SRM method was set by recording the retention time of two peptides for each selected protein and for glyceraldehyde 3-phosphate dehydrogenase—chosen as housekeeping protein—in a representative CGN sample, and by selecting five diagnostic precursor-to-product ion transitions for each target peptide under the above-reported liquid chromatography conditions. The selected ion transitions, together with the retention time and the instrumental settings used in the acquisition method, are reported in Supplementary Table S1.

The Skyline software [36] was used to assess the relative abundance of each peptide, by calculating the area under the curve of the corresponding chromatographic peak. Obtained values were then normalized to the sum of the values of the two glyceraldehyde 3-phosphate dehydrogenase peptides. To compare the abundance of each protein between PrP-Tg and PrP-KO neurons, all area-under-the-curve values were normalized to the mean value of PrP-Tg samples. The above-described SRM workflow is schematically summarized in Supplementary Fig. S2.

Western Blot Analysis and Antibodies

To carry out Western blot analysis, 10 μg of total proteins diluted in reducing sample buffer was firstly subjected to SDS-PAGE—using Mini-Protean TGX precast gels (4–15%; Bio-Rad Laboratories)—and then electrophoretically transferred (1 h, 350 mA) onto polyvinylidene difluoride membranes (0.22 μm pore size; Bio-Rad Laboratories). After staining with Coomassie brilliant blue (Sigma) to ensure equal protein loading and transfer, and destaining with methanol, membranes were incubated (1 h, RT) in a blocking solution [5% (*w*/*v*) non-fat dry milk (Bio-Rad Laboratories) in PBS added with 0.1% (*w*/*v*) Tween-20 (PBS-T)], and then probed (overnight, 4 °C) with the desired primary antibody diluted in the blocking solution. After three washings with PBS-T, membranes were treated (1 h, RT) with horseradish peroxidase-conjugated anti-mouse or anti-rabbit IgG (Santa Cruz Biotechnology, cat. no. sc-2005 and sc-2004, respectively) diluted (1:3000) in the blocking solution. Immunoreactive bands were visualized and digitalized by means of an UVItec imaging system (Eppendorf), using an enhanced

chemiluminescence reagent kit (EMD Millipore). For densitometric analyses, the intensity of each immunoreactive band was normalized to the optical density of the corresponding Coomassie blue-stained lane [37].

The following primary monoclonal antibodies were used (dilutions are in parentheses): mouse anti-Rab3a (1:10,000; Synaptic Systems, cat. no. 107111); rabbit anti-Rab7a (1:1000; Cell Signaling Technology, cat. no. 9367); rabbit anti-Rab11b (1:1000; Cell Signaling Technology, cat no. 5589); mouse anti-VAMP2 (1:5000; Synaptic Systems, cat. no. 104211); mouse anti-Syt1 (1:1000; Synaptic Systems, cat. no. 105011); mouse anti-phosphorylated (on Ser133) Creb1 (1:1000; Cell Signaling Technology, cat. no. 9196s); rabbit anti-Creb1 (1:1000; Cell Signaling Technology, cat. no. 9197s).

Quantitative Real-Time PCR (qRT-PCR)

Total RNA was purified after CGN lysis in 500 μl of TRIzol Reagent (Thermo Fisher Scientific, cat. no. 11596026), using the standard phenol–chloroform extraction and isopropanol precipitation. First-strand cDNA was synthesized starting from 1 μg of total RNA in a total volume of 20 μl, using oligo-dT as primers and SuperScript II reverse transcriptase (Thermo Fisher Scientific, cat. no. 18064014), following manufacturer's instructions. EvaGreen technology was applied for all assays using the ABI 7500 Standard qRT-PCR System (Thermo Fisher Scientific). Reactions were performed in a final volume of 20 μl, including 4 μl of HOT FIRE Pol EvaGreen qPCR Mix Plus (Solis BioDyne), 0.4 μl of reverse primer (10 μM), 0.4 μl of forward primer (10 μM), 1 μl of the (20 ng/μl) cDNA template, and 14.2 μl of water. Primer sequences for each gene (Supplementary Table S2) were chosen using the Primer3Plus software. After a 15-min denaturation step at 95 °C, the PCR program was as follows: 95 °C, 15 s; 60 °C, 20 s; 72 °C, 20 s (40 cycles). The reaction was terminated by a dissociation step consisting in 95 °C, 15 s; 60 °C, 60 s; 95 °C, 15 s; and 60 °C, 15 s. mRNA levels were measured according to the $\Delta\Delta C_t$ method and using TATA-box binding protein as housekeeping gene.

Computational Biology

Gene ontology enrichment analysis was performed using the web-based Gene SeT AnaLysis Toolkit (http://www.webgestalt.org/option.php) [38], correcting for multiple tests using the Benjamini–Hochberg procedure to assess the false discovery rate.

The oPOSSUM web-based system (v 3.0) [39] and the Jaspar database [40] were used for identifying over-represented, conserved binding sites for transcription factors in the promoter region of the target genes. The following parameters were used: minimum specificity, 8 bits; conservation cut-off, 0.40; matrix score ≥ 80%; 5000 bp upstream and 5000 bp downstream the transcription start site. The Z-scores, calculated considering all genes in the oPOSSUM database as background, were used to filter results. The chromatin immunoprecipitation atlas (http://chip-atlas.org), covering almost all public chromatin immunoprecipitation-sequencing data submitted to the Sequence Read Archives in NCBI, DDBJ, or ENA databases, was used to further filter the oPOSSUM-based results. In this second analysis round, only chromatin immunoprecipitation-validated interactions between target genes and transcription factors were considered.

Statistical Analyses

All data are reported as mean ± standard error of the mean (SEM) or standard deviation (SD), as indicated in the figure legends. Quantification of glutamate release, SV recycling assays, untargeted proteomic analysis, and qRT-PCR were performed using three, while SRM and Western blot experiments using six, distinct CGN cultures for each PrP genotype (biological replicates), respectively. For SV recycling assays and qRT-PCR analysis, two and three technical replicates were made for each biological replicate, respectively. In these cases, the mean value of the technical replicates for each biological replicate was firstly calculated, and data were then reported as the mean of the average biological replicate values. Statistics was based on two-tailed *Z* test, Student's *t* test, or one-way ANOVA, depending on the experiment, as indicated in the figure legends, with a p value < 0.05 being always considered statistically significant.

Results

PrP^C Contributes to Ensure Efficient Synaptic Transmission

To assess the potential contribution of PrP^C in synaptic signaling, we firstly employed an MS-based approach to quantify the release of glutamate by primary CGN isolated from co-isogenic PrP^C-expressing (PrP-Tg) and PrP-KO mice, exposed to a depolarizing stimulus (high $[K^+]$). Figure 1 reports that PrP-KO CGN released a lower (around 40%) glutamate amount than PrP-Tg neurons. Glutamate originated from presynaptic activity, as in both CGN types its secretion was completely abrogated by the exocytosis blocker botulinum toxin D (BoNT/D, Fig. 1). Supplementary Fig. S3 validates the toxin's metalloprotease activity, in light of the reported decreased amount of full-length VAMP2, one major component of SV fusion machinery [41].

A further proof for PrP^C ability to govern synaptic functions was obtained by following the SV exo-endocytotic cycle. This test was accomplished by depolarizing neurons (as above) in the presence of an antibody recognizing a luminal domain of the SV-transmembrane, Ca^{2+}-binding protein synaptotagmin 1 (Syt1) [33], which critically serves in the

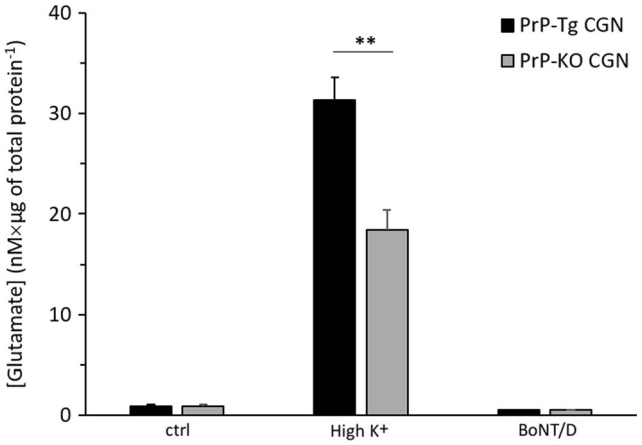

Fig. 1 PrP^C regulates glutamate release from primary CGN under depolarizing conditions. 96 h after plating, cerebellar granule neurons (CGN) expressing (PrP-Tg, black bars), or not (PrP-KO, gray bars), PrP^C, were depolarized by incubation (5 min) in a medium containing 60 mM KCl (high [K^+]), or maintained in a non-depolarizing medium (cntr). As a negative control, CGN were pre-incubated (30 min) with botulinum toxin (BoNT/D, 10 nM)—an inhibitor of the synaptic vesicle (SV) recycling process—before the depolarizing step. Shown glutamate concentrations, quantified by LC-MS in the CGN bathing medium at the end of the depolarization step (as described in the "Materials and Methods" section), and normalized to the total protein content of the corresponding CGN lysate, clearly indicate an approximately 40% reduction of glutamate secretion by PrP-KO neurons. This result highlights a positive regulation by PrP^C on glutamate release. Little or no glutamate amounts were detected in non-depolarized, and in BoNT/D-treated (see also Supplementary Fig. S3), neurons. Data are mean ± standard error of the mean (SEM), $n = 3$ for each condition and PrP genotype; $^{**}p < 0.001$, Student's t test

synchronous-evoked SV exocytosis [42]. The target domain is exposed to the extracellular space, and hence to the added antibody, after the SV membrane merges into the plasma membrane, and is subsequently internalized in the vesicle recycling process. Notably, equal Syt1 amounts were present in both CGN types (Supplementary Fig. S4). Figure 2 shows the Western blot of neurons, performed by labeling the cell-sequestered antibody to Syt1 with anti-mouse IgG (panel a, lanes 9–14), and the corresponding densitometric quantification (panel b), demonstrating that PrP-KO CGN accumulated around 60% less Syt1 than PrP-Tg neurons. Figure 2 also shows that the presence of BoNT/D strongly reduced the intensity of the immuno-signal of the antibody to Syt1 (panel a, lanes 1–2)—confirming the functional dependence of Syt1 internalization from SV cycle—while lack of signals observed in the absence of the anti-Syt1 antibody (panel a, lanes 3–8) excluded any cross-reactivity by the anti-mouse IgG. Taken together, results of Figs. 1 and 2 demonstrate that the absence of PrP^C impaired glutamate release and SV recycling.

Proteomic Analysis by Untargeted MS

Next, to identify possible molecular mechanisms for the dysregulated glutamate secretion by PrP-KO CGN, we carried out an unbiased large-scale proteomic comparison of the two CGN types. This choice also stemmed from our previous findings showing changes in the membrane proteome of PrP-KO CGN relative to wild-type neurons [43]. As schematically illustrated in Supplementary Fig. S1, protein expression patterns were examined using isotopomeric dimethyl tags with different mass to label peptides derived from trypsin-digested PrP-Tg and PrP-KO CGN lysates [34], followed by untargeted LC-MS/MS analysis of three different replicates. Replicates were obtained by mixing together two differently labeled peptide pools originating from PrP-Tg and PrP-KO samples. The following number of identified peptides and protein groups, respectively, was obtained (Fig. 3a): 3379 and 480 for replicate 1; 2797 and 458 for replicate 2; 3248 and 493 for replicate 3. To note that, out of the total 606 identified protein groups (indicated as multi-consensus report), 369 were those in common to all replicates according to the Venn diagram (Fig. 3b). Gene ontology analysis indicated that MS-identified data in the three replicates were homogenous in terms of classes belonging to the three gene ontology categories, i.e., "Cellular component," "Molecular function," and "Biological process" (Supplementary Fig. S5). This result also indicates that the biological variability intrinsic to primary cultures impacted in a minimal, if none, manner on the reported experiments, highlighting the robustness of the analysis.

To refine further the proteomic analysis, the 369 proteins identified in both CGN types were statistically compared for their abundance using a two-tailed Z test (with a p value < 0.05 being considered acceptable). Based on the difference in protein expression calculated as the mean ratio of PrP-KO over PrP-Tg CGN values, Table 1 reports that, compared to PrP-Tg neurons, 26 proteins of PrP-KO CGN were at least 1.3-fold downregulated (i.e., the ratio being < 0.77), while Supplementary Table S3 shows that 22 were those at least 1.3-fold upregulated (i.e., the ratio being > 1.30). Importantly, gene ontology analysis of the under-represented proteins in PrP-KO CGN not only highlighted that "Mitochondrion" (by 28%) and "Neuron" (by 22%) were the categories to which these proteins most significantly belonged but also revealed a strong correlation between the above proteins and categories such as "Presynapse" (by 15%), "Transport vesicle" (by 11%), "Secretory vesicle" (by 13%), and "Synaptic/exocytic vesicle" (by 11%) (Fig. 3c and Supplementary Table S4). This in silico approach thus indicates a close correlation between the clear synaptic phenotype observed in PrP-KO neurons and the downregulation of proteins involved in (pre)synaptic physiology. In particular, downregulated proteins comprised seven documented regulators of vesicle trafficking and release, namely, four Ras-related in brain [(Rab)1a [44], Rab3a [45], Rab7a [46], Rab11b [47]], syntaxin-1B (Stx1b [48]), synaptogyrin 3 (Syngr3 [49]), and the isoform 2 of α-synuclein [50]. Conversely, Supplementary

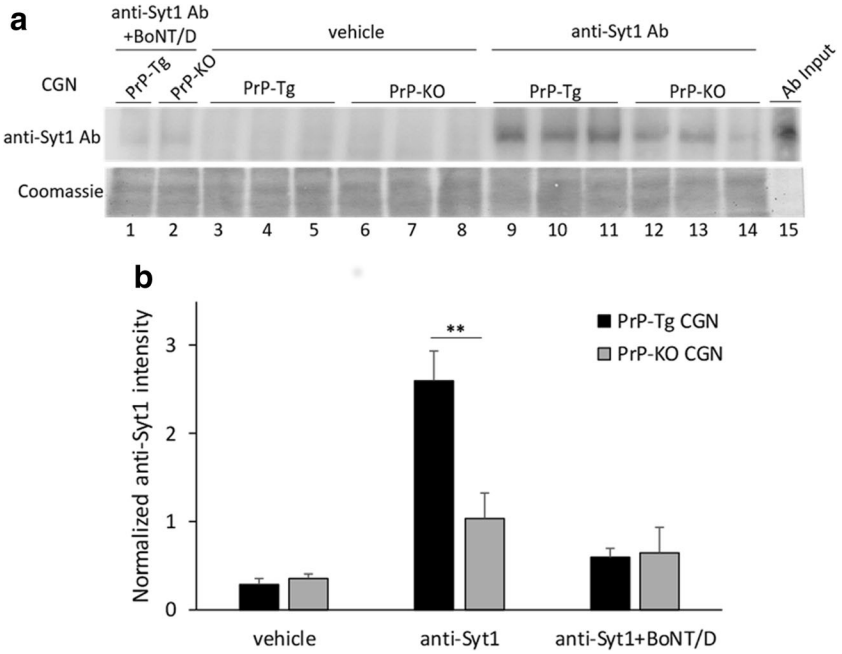

Fig. 2 PrP^C regulates recycling of SVs in primary CGN. **a** The upper part of the panel reports a representative Western blot of primary PrP-Tg and PrP-KO CGN incubated (20 min) in a depolarizing medium (containing 60 mM KCl) that promotes exo-endocytosis of SVs. The endocytic process was followed in the presence (lanes 9–14), or in the absence (lanes 3–8), of a mouse monoclonal antibody (Ab) to the luminal domain of the SV membrane-located synaptotagmin 1 (Syt1). To quantify Syt1 internalization, neurons were lysed, subjected to SDS-PAGE (under non-reducing conditions), and finally processed by Western blot, using a horseradish peroxidase-conjugated antibody recognizing mouse IgG (i.e., the internalized anti-Syt1 antibody). As a negative control, before incubation with the anti-Syt1 antibody, neurons were pre-treated with BoNT/D (10 nM, 30 min, lanes 1–2). A sample of anti-Syt1 antibody (10 ng) was also loaded in the gel as positive control (Ab input, lane 15). Coomassie blue staining of membranes (shown in the lower part of the panel) was performed to verify equal protein loading and blotting efficiency. **b** The bar diagram reports the densitometric analysis of immunoreactive bands in PrP-Tg (black) and PrP-KO (gray) samples under the different conditions, normalized to the optical density of the corresponding Coomassie blue-stained lane. Quantification of the internalized anti-Syt1 antibody in CGN with the two genotypes clearly shows that the absence of PrP^C hampered SV internalization (around 60% reduction), while the anti-Syt1 signal in BoNT/D-treated neurons approximates the background signal detected in vehicle-treated controls. Data are mean ± SEM, $n = 3$ for each condition and PrP genotype; $^{**}p < 0.01$, Student's t test. For other details, see the legend to Fig. 1

Table S3 shows that the upregulated group contained no protein linked to these processes. In addition, although other proteins participating in SV dynamics were successfully quantified (not shown), including the previously cited Syt1, there was no significant difference in their amounts present in the two CGN types. Taken together, these data argue that specific proteins acting on the overall SV physiology are under the control of PrP^C.

Data Validation by Targeted MS and Quantitative (q) RT-PCR

Because the involvement of Rab1a, Rab3a, Rab7a, Rab11b, Stx1b, and Syngr3 in SV physiology (Table 1; Fig. 3c and Supplementary Table S4) clearly fitted with the PrP-KO phenotypes emerged from the functional tests (Figs. 1 and 2), these proteins were examined by a targeted SRM-based proteomic strategy, using six CGN cultures for each PrP genotype (Supplementary Fig. S2). Analysis included the downregulated cluster of those proteins referred to as "nerve ending signal proteins" [51] [i.e., neuromodulin (Gap43), brain acid soluble protein 1 (BASP1), and myristoylated alanine-rich C-kinase substrate (MARCKS)-related protein (Marcksl1); Table 1], whose altered expression has been already reported in some PrP-KO cell lines [52], and aspartate aminotransferase 1 (Got1) that, together with Syngr3, Table 1 indicates as the most under-represented protein evidenced by untargeted MS. The SRM methodology quantifies target proteins with high efficiency and reproducibility [53] through the quantification of at least two in silico selected proteotypic peptides for each protein [54] (Supplementary Table S1 and Fig. S6). Figure 4 confirms the reduced quantity of Gap43, BASP1, Marcksl1, and Got1 in PrP-KO CGN also on the basis of the SRM analysis. Most importantly, however, SRM data of Fig. 4 demonstrate that the absence of PrP^C also lowers the abundance of Rab3a, Stx1b, and Syngr3, on the one hand, and Rab1a, Rab7a, and Rab11b, on the other hand, recognizing the functional link of PrP^C to the presynaptic release apparatus [45, 48, 49] and vesicle transport [44, 46, 47], respectively. Notably, the Western blot analysis of Supplementary Fig. S7 further supports the contention that PrP^C absence downregulated Rab3a, Rab7a, and Rab11b in PrP-KO CGN compared to PrP-Tg counterparts.

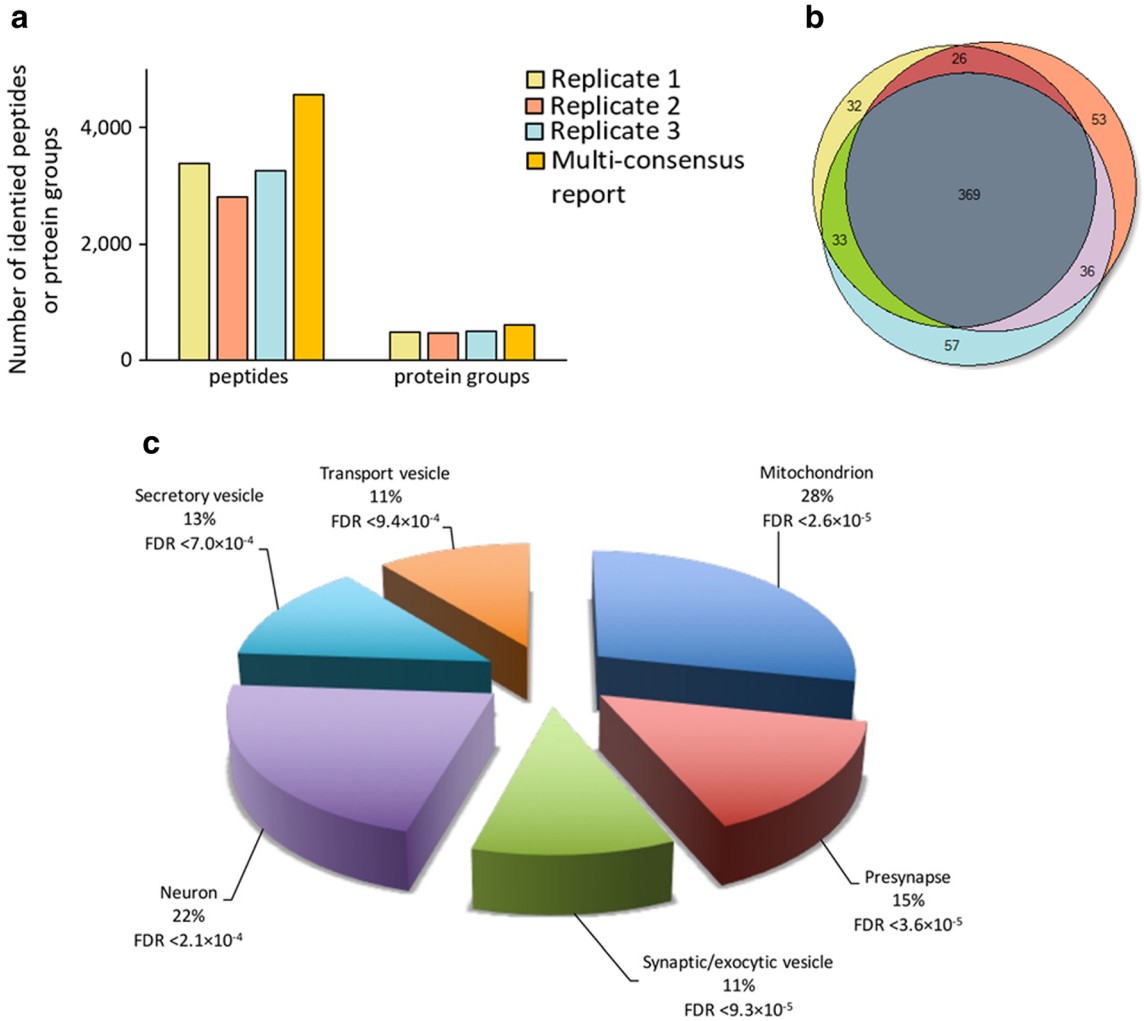

Fig. 3 Protein identification by untargeted MS analysis. An untargeted MS-based approach was used to obtain the quantitative proteome profiling of PrP-Tg and PrP-KO CGN. **a** The bar diagram reports the number of peptides and protein groups belonging to each replicate (1–3), or all of them together (multi-consensus report), as resulting from analysis of untargeted MS data (for details on the procedure, see also Supplementary Fig. S1). **b** The Venn diagram reports the number of protein groups identified in each replicate, and whether they are unshared (yellow, 1; orange, 2; pale blue, 3), or in common either between two replicates (green, 1 and 3; violet, 2 and 3; red, 1 and 2) or among all replicates (gray). **c** The pie chart reports the gene ontology refinement analysis of under-represented proteins in PrP-KO CGN. All related categories of gene ontology, identified by the Gene SeT AnaLysis Toolkit, are reported in Supplementary Table S4. Geneset hits—with a false discovery rate (FDR) < 0.001—were clustered into the six displayed functional groups, and reported as percentage of the total overlapping gene hits in such clustered categories using the lowest FDR value

qRT-PCR was then applied to understand whether such a PrP^C-dependent regulation of the abundance of SV proteins originated from transcriptional control. Figure 5 reports that, similar to proteomic data, mRNAs of all the corresponding genes were significantly lower (by 25–55%) in PrP-KO CGN than in PrP-Tg neurons. Instead, no difference in Syt1 transcripts was detected in the two CGN types, endorsing previous MS (data not shown) and Western blot (Supplementary Fig. S4) analyses. These results indicate that the reduced protein expression observed in the absence of PrP^C arose from transcriptional (and/or RNA processing) alterations, rather than from defects in protein synthesis and/or turnover.

Finally, we searched for over-represented binding sites for transcription factors in the promoter region of the altered genes to understand whether all these genes were controlled by common transcription factors. To this end, we performed a computational approach based on sequence analysis and interactome (chromatin immunoprecipitation-based) databases. As reported in Supplementary Fig. S8 and Table S5, this in silico study identified Creb1, Nr3c1, and Sp1 as the statistically most enriched transcription factors for the target genes. In particular, Creb1 was found to transcriptionally regulate five out of the six downregulated target genes, with the highest Z-score among all considered factors (Supplementary Table S5 and Fig. S9). These results, and the notion that Creb1 is a possible downstream target of PrP^C-dependent signaling pathways [55], fostered further investigations aimed at verifying the phosphorylated (active) state of Creb1, under basal (non-

Table 1 Downregulated proteins in primary PrP-KO CGN

Protein name	Gene name	PrP-KO CGN/PrP-Tg CGN mean ratio ± SD	*p* value	Gene ontology category: biological process or molecular function
Synaptogyrin-3	Syngr3	0.62 ± 0.14	1.04×10^{-4}	Positive regulation of transporter activity
Aspartate aminotransferase, cytoplasmic	Got1	0.62 ± 0.26	3.28×10^{-2}	Amino acid biosynthesis
Neuromodulin	Gap43	0.66 ± 0.14	2.14×10^{-4}	Differentiation, growth regulation, neurogenesis
Syntaxin-1B	Stx1b	0.68 ± 0.12	6.00×10^{-5}	Neurotransmitter transport, transport
Brain acid soluble protein 1	Basp1	0.68 ± 0.14	3.82×10^{-4}	Negative regulation of transcription
MARCKS-related protein	Marcksl1	0.68 ± 0.20	1.38×10^{-2}	Positive regulation of cell proliferation
Ras-related protein Rab-1A	Rab1a	0.68 ± 0.14	6.35×10^{-4}	Autophagy, ER-Golgi transport, protein transport, transport
Succinyl-CoA:3-ketoacid coenzyme A transferase 1, mitochondrial	Oxct1	0.69 ± 0.19	1.23×10^{-2}	Transferase
Prohibitin-2	Phb2	0.70 ± 0.16	7.89×10^{-3}	Transcription, transcription regulation
Ras-related protein Rab-3A	Rab3a	0.70 ± 0.12	1.90×10^{-4}	Exocytosis, protein transport, transport
Tubulin beta-4B chain	Tubb4b	0.71 ± 0.12	4.83×10^{-4}	Microtubule-based process
Ras-related protein Rab-11B	Rab11b	0.72 ± 0.23	3.80×10^{-2}	Protein transport, transport
Histone H2B type 1-F/J/L	Hist1h2bf	0.72 ± 0.11	5.66×10^{-5}	DNA binding
ATP synthase subunit g, mitochondrial	Atp5l	0.72 ± 0.15	2.73×10^{-3}	ATP synthesis coupled proton transport
Acetyl-CoA acetyltransferase, mitochondrial	Acat1	0.72 ± 0.08	1.56×10^{-7}	Metabolic process
Myristoylated alanine-rich C-kinase substrate	Marcks	0.72 ± 0.18	1.13×10^{-2}	Actin-binding, calmodulin-binding
ATP synthase F(0) complex subunit B1, mitochondrial	Atp5f1	0.73 ± 0.12	5.25×10^{-4}	ATP synthesis coupled proton transport
Ras-related protein Rab-7a	Rab7a	0.73 ± 0.32	2.30×10^{-2}	Early endosome to late endosome transport
Synaptic vesicle membrane protein VAT-1 homolog	Vat1	0.74 ± 0.13	1.35×10^{-3}	Negative regulation of mitochondrial fusion
Isoform 2 of Alpha-synuclein	Snca	0.74 ± 0.14	5.95×10^{-3}	Regulation of dopamine release and transport
Pyruvate kinase PKM	Pkm	0.74 ± 0.20	4.11×10^{-2}	Glycolytic process
ATP synthase subunit alpha, mitochondrial	Atp5a1	0.75 ± 0.08	7.82×10^{-7}	ATP synthesis coupled proton transport
60S ribosomal protein L18	Rpl18	0.75 ± 0.17	2.99×10^{-2}	Translation
Malate dehydrogenase, mitochondrial	Mdh2	0.75 ± 0.09	1.88×10^{-5}	Tricarboxylic acid cycle
Stathmin	Stmn1	0.76 ± 0.17	1.75×10^{-2}	Regulation of microtubule polymerization
Stress-70 protein, mitochondrial	Hspa9	0.76 ± 0.15	1.65×10^{-2}	Chaperone

Among the 369 proteins identified in both PrP genotypes, only proteins whose PrP-KO/PrP-Tg expression ratio was < 0.77 (p value < 0.05, two-tailed Z test) are reported. Denomination of proteins and genes is reported in the first two columns, while the last column reports the UniProtKB-assigned biological process or molecular function gene ontology category

stimulated) conditions, in the two CGN types. By reporting the Western blot-based quantification of phosphorylated Creb1, Fig. 6 shows that this transcription factor was significantly less (by around 50%) active in PrP-KO CGN than in PrP-Tg neurons. This finding further corroborates the possibility that Creb1 takes part in a PrP^C-dependent transcriptional control of the examined SV-connected proteins.

Discussion

In an effort to delineate the pathophysiology of PrP^C at synapses, our work has combined functional tests with proteomic and qRT-PCR approaches to examine primary PrP^C-expressing (PrP-Tg), and PrP-KO, CGN cultures. Compared to PrP-Tg CGN, LC-MS/MS analysis identified multifactorial changes in the PrP-KO proteome. This result suggests a complex regulation brought about by PrP^C, which however is consistent with the rich interactome and the governance of multiple signaling pathways that have been attributed to the protein [11–15]. Among the several differentially expressed proteins in PrP-KO CGN, we concentrated on the downregulated ones serving in vesicular trafficking (i.e., Rab1a, Rab7a, and Rab11b) and neurotransmitter release (i.e., Rab3a, Stx1b, and Syngr3), which received validation by SRM and mRNA analyses. The study demonstrated that the lower amount of proteins, and of their gene transcripts, in PrP-KO CGN stringently correlated with the robust diminution of SV cycling, and with an equally poor glutamate release, observed in these cells.

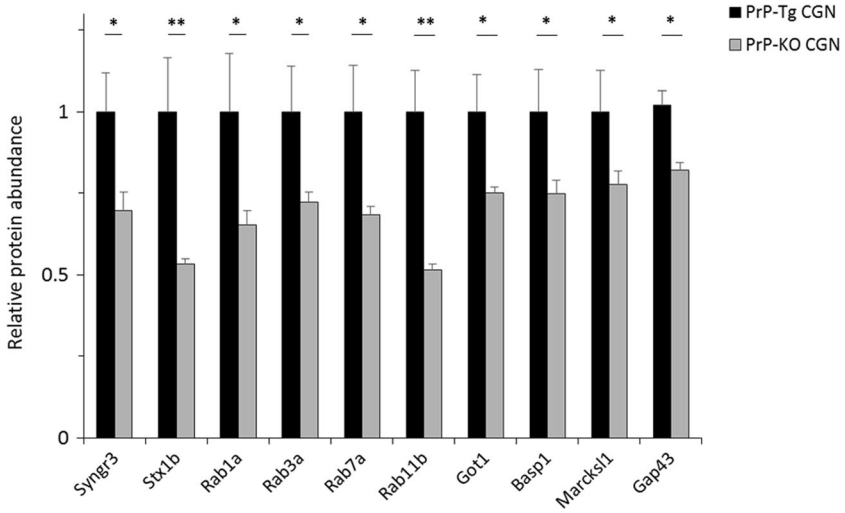

Fig. 4 Selected reaction monitoring validates the PrP^C-dependent abundance of proteins involved in SV dynamics. Proteins involved in SV dynamics that—by untargeted proteomic analysis—showed lower abundance in PrP-KO CGN compared to PrP-Tg neurons (i.e., synaptogyrin 3 (Syngr3), syntaxin-1B (Stx1b), Rab1a, Rab3a, Rab7a, Rab11b) were subjected to validation by selected reaction monitoring (SRM). Marcksl1, BASP1, and Gap43 were similarly screened, owing to the hypothesized metabolic link with PrP^C, while Got1 was examined because, together with Syngr3, it was indicated by large-scale proteomics as the most downregulated protein in PrP-KO CGN. The bar diagram, reporting the relative protein quantity in PrP-KO neurons (gray) with respect to values found in the PrP-Tg counterpart (black), confirms that PrP^C positively regulates the abundance of all the analyzed proteins. Data are mean ± SEM; $n = 6$ for each PrP genotype. $*p < 0.05$; $**p < 0.01$, Student's t test. For other details, see Supplementary Figs. S2 and S6

These data may thus support that a key function of PrP^C in neurons is to ensure highly efficient neurotransmitter secretion, as also suggested by previous works that, through different methodologies, highlighted the capacity of PrP^C to potentiate synaptic release and plasticity [24–30]. Relating to the accomplishment of this task at presynapses, our results agree with studies on glutamatergic neuromuscular junctions of *Drosophila melanogaster* (which harbors no mammalian PrP ortholog) expressing transgenes for the murine wild-type PrP^C, or the disease-related PrP^{P101L} mutant. Indeed, comparison of neuromuscular junction morphology and locomotor activity [29, 56], or of the electrophysiological patterns [29], of the two transgenic larvae, allowed concluding that PrP^C positively regulated presynaptic activity by affecting the size and release probability of SVs, as well as the number, or function, of active zones. However, despite earlier proposals on PrP^C capacity to control gene expression (see below), to the best of our knowledge for the first time our results hold that PrP^C preserved appropriate synaptic signaling through the modulation of genes implicated in SV trafficking and exocytosis.

Considering the four identified Rab proteins, they belong to the large Ras-like superfamily of small GTPases

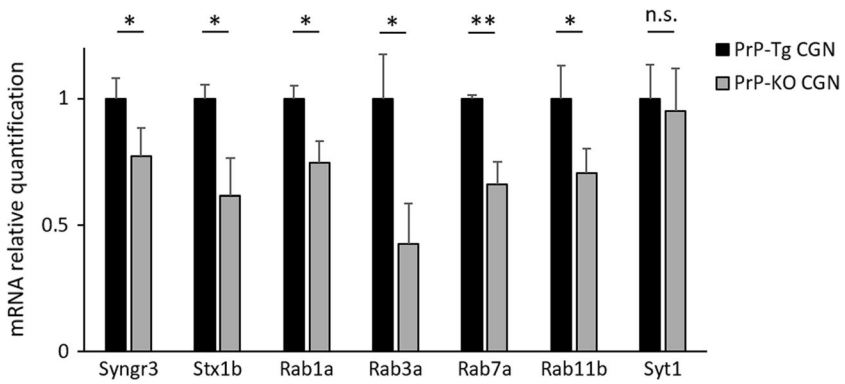

Fig. 5 qRT-PCR validates the transcriptional regulation by PrP^C of proteins involved in SV dynamics. RNA purified from CGN was retrotranscribed, and obtained cDNA was subjected to qPCR using primer pairs (Supplementary Table S2) specific for each target gene (i.e., expressing synaptogyrin 3 (Syngr3), syntaxin-1B (Stx1b), Rab1a, Rab3a, Rab7a, Rab11b, Syt1), and the housekeeping gene (TATA-box binding protein). The mRNA amount for each target gene in PrP-Tg (black bars) or PrP-KO CGN (gray bars) was normalized to the mRNA amount of the housekeeping gene in the corresponding sample, and reported after further normalization to PrP-Tg values. qRT-PCR indicates that Syngr3, Stx1b, Rab1a, Rab3a, Rab7a, and Rab11b are transcriptionally downregulated in PrP-KO CGN compared to PrP-expressing neurons, while—consistent with MS (not shown) and Western blot (Supplementary Fig. S4) data—Syt1 is equally expressed in both PrP genotypes. Data are mean ± SD; $n = 6$ for each PrP genotype; $*p < 0.05$; $**p < 0.01$; n.s., non-significant, Student's t test

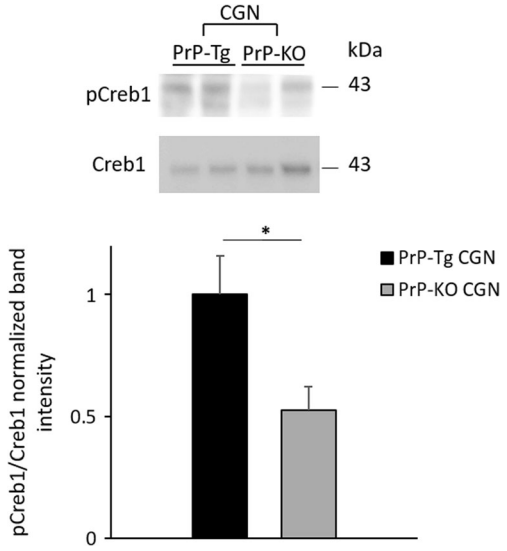

Fig. 6 PrP^C controls Creb1 activation in CGN under basal conditions. Proteins (10 μg) from PrP-Tg or PrP-KO CGN were analyzed by Western blot using a monoclonal antibody to phospho-Creb1 (Ser133, pCreb1) or total Creb1. The upper panel shows a representative Western blot, while the bar diagram in the lower panel shows the ratio between pCreb1 and Creb1 band intensity, each of which was previously normalized to the corresponding Coomassie-stained lane. Reported data (mean ± SEM; $n = 6$ for each PrP genotype) were further normalized to the mean value of PrP-Tg samples; $^*p < 0.05$, Student's t test

performing fundamental tasks in vesicular dynamics, from exocytosis and endocytosis, to autophagy [57]. Among them, Rab3a is the one apparently associated only to SVs [58]. Rab3a, which forms a trimeric complex with core proteins of the active zone deputed to docking and priming SVs for exocytosis and to recruit voltage-gated Ca^{2+} channels [45], is also implicated in some forms of long-term potentiation [59] and in the control of the active zone protein composition [60]. Instead, each of the other three Rab proteins regulates specific steps of vesicle transport. Briefly, Rab1a mediates membrane trafficking between the endoplasmic reticulum and Golgi apparatus—and lipid and protein transport thereof—although other important functions are now emerging [44]. Normally localized to late endosomes, Rab7a controls endosomal maturation up to the fusion of late endosomes with lysosomes [46], and endosomal recruitment into (fast) retrograde axonal transport [61]. Finally, Rab11b is involved in the early endocytic pathway and directs cycling vesicles to the plasma membrane [47]. Conversely, Syngr3 and the plasma membrane SNARE protein Stx1b belong to the SV fusion apparatus. Of the two, transmembrane Syngr3 localizes exclusively to SVs, but its role in the fusion mechanism is not yet fully clarified [49]. However, it has been recently reported that the Alzheimer's disease-associated hyperphosphorylated tau protein binds to Syngr3 under pathological conditions, provoking defective SV transport and release [62]. As to Stx1b, its prominent implication in spontaneous and evoked vesicle exocytosis in fast synaptic transmission is well recognized [63]. Mechanistically, the protein associates with VAMP2 and SNAP-25 to form the trans-SNARE complex that, with the essential intervention of other partners (including the Ca^{2+}-activated Syt1), mediates SV fusion after voltage-gated Ca^{2+} channels respond to an action potential allowing Ca^{2+} inflow [64]. Of interest, downregulation of Stx1b was already noticed in a previous large-scale analysis of PrP-KO CGN membrane proteome compared to the wild-type counterpart [43], while Rab7a was identified as a PrP^C interactor in different neuronal lines [65].

In light of the above-sketched functions, one may conclude that the compromised glutamate secretion by PrP-KO CGN originates from defects in the presynaptic fusion apparatus, and/or in SV recycling that would reduce the pool of releasable vesicles. It is worth underlining, however, that other proteins controlling SV exo-endocytosis coupling, including critical participants in the diverse neuronal endocytic routes and the multiple regulators and effectors of the Rab family activity [66], could have escaped quantification by the employed MS-based approach. Another issue to consider in the PrP^C-synapse relationship is whether a differential voltage-gated channel-mediated Ca^{2+} entry contributed to dysregulate glutamate secretion in PrP-KO CGN, particularly in light of current evidence supporting a contribution of PrP^C in the control of neuronal Ca^{2+} homeostasis [67, 68]. On this, our examination of local Ca^{2+} fluxes [32, 69] argues against the possibility that a reduced voltage-gated channel-dependent Ca^{2+} entry could have affected SV release in the absence of PrP^C, and/or the previously proposed direct requirement of PrP^C for Ca^{2+}-dependent glutamatergic transmission in CGN [70].

Unsurprisingly, dysfunction of most of the here-considered proteins has been connected to neurodegenerative processes. For example, accumulation of PrP^{Sc} was related, among other synaptic proteins, to a reduced presence of Stx1b and Rab3a (the latter also showing abnormal metabolism) [71, 72]. PrP^{Sc} accumulation was also linked to a disrupted membrane association [73], and cell localization [74], of Rab7, affecting lysosomal degradation and retrograde axonal transport, respectively. Likewise, a human disease-related PrP mutant provoked the overexpression of an inhibitor of membrane-associated Rab activity, which led to a diminished functional amount of Rab11b [75]. On the other hand, while Rab7a mutants have been linked to peripheral neuropathy [46], and Stx1b mutants and polymorphisms to fever-associated epilepsy syndromes [76] and Parkinson's disease [77], respectively, it has also been reported that excessive Parkinson's disease-related α-synuclein deregulated Rab1a, and, vice versa, that increased Rab1a activity opposed α-synuclein toxicity [44].

The here-disclosed genetic association of PrP^C to Rab family members, and/or to the other proteins intimately involved in the SV fusion machinery, may thus provide important insight in the molecular connection between a compromised PrP^C behavior and synaptic dysregulation. In this regard, it is also good to remind that the binding to PrP^C of prion-,

Aβ-, or prefibrillar α-synuclein-oligomers results in the activation of common synapto-toxic pathways, comprising overactivation of the Src-related kinase Fyn and of NMDA-sensitive ionotropic glutamate receptor channels, and impairment of Ca^{2+} homeostasis and synaptic plasticity [4, 20, 21, 78–82]. The emerging picture is therefore consistent with the possibility that signaling routes, which are normally coupled to PrP^C [15, 83–86], become compromised as interaction with the mentioned oligomeric species induces loss of PrP^C normal behavior, or acquisition of neurotoxic functions by PrP^C. Hence, were noxious oligomers also disrupting PrP^C genetic control over presynaptic physiology, new possibilities will be offered for protective therapies targeting synaptic dysfunctions, which are the established early pathogenic feature in several neurodegenerative disorders [79, 87–89].

The possibility that PrP^C could regulate protein expression has already been tackled by large-scale transcriptomic and proteomic approaches, which, however, have provided contradictory results. From the one hand, no difference was observed in the proteome, or transcriptome, of wild-type and PrP-KO mouse brains [52, 90, 91]. Instead, large-scale mRNA analysis [92], and global [52, 93, 94], or membrane [43], proteome profiling of primary cells and/or cell lines, highlighted the involvement of PrP^C in controlling the expression of proteins governing various cellular events. Proteomic and qRT-PCR data of the present report are thus in accordance with the latter findings, having underscored that PrP^C intervenes in the expression of proteins involved in synaptic transmission.

Yet, a major unsolved question concerns the mechanism(s) by which such a regulation is achieved. A step forward on this issue may be provided by the here-employed bioinformatic approach coupled to biochemical analysis, which proposes that PrP^C operates on gene transcription via (at least) Creb1-mediated control. Remarkably, Creb1, which is activated by several signaling cues, including cAMP, Ca^{2+}, and different phosphorylation-based cascades [95], has been repeatedly implicated in synaptic physiology [96]. Likewise, a recurrent notion in PrP^C biology conceives that, as a component of cell surface multi-receptor platforms, PrP^C affects downstream signaling events [11] that may eventually culminate in the regulation of gene transcription [55]. On this, pertinent examples are the regulation by PrP^C of Ca^{2+} homeostasis [67, 68] and various signaling pathways, including those involving Fyn, cAMP-dependent protein kinase A, and the Akt-PI3-, Erk1/2-, or p38-dependent axes [11]. Importantly, artificial (antibody-mediated) stimulation of PrP^C leads to Creb1 activation through Fyn and/or PI3K cascades in immortalized neuronal cell lines [55].

Taken together, our and past findings suggest a possible involvement of PrP^C in the expression of pre-synaptic proteins involved in SV physiology via Creb1 regulation. Undoubtedly, however, in light of the panoply of signaling pathways converging on Creb1, and the similarly large spectrum of routes putatively controlled by PrP^C, deeper investigations are required to fully elucidate the intermediate(s) between (cell surface) PrP^C and activation of (nuclear) Creb1 in neurons.

Finally, because this work centered on PrP-KO paradigms, one may ask the question of how the profoundly compromised glutamate secretion observed in PrP^C-deprived CGN can be compatible with the lack of gross cognitive and behavioral phenotypes in PrP-KO animals [9, 10]. A plausible answer could refer to the reported capacity of PrP^C to act post-synaptically in defending neurons from Ca^{2+}-overload excitotoxicity. Indeed, PrP^C depresses the activity of NMDA–, AMPA–, and kainate–glutamate receptor subtypes [85, 86], which might also explain why PrP^C-expressing animals are more protected than PrP-KO counterparts from depressive-like syndrome, ischemia, and kainate-induced seizures involving ionotropic glutamate receptor channels [97–101]. In this scenario, the increased postsynaptic Ca^{2+} influx mediated by these channels in the absence of PrP^C could preserve synaptic signaling by compensating for the reduced glutamate secretion by PrP-KO CGN presynapses. However, such a counterbalance may no longer hold upon aging, and/or stress, whereby those behavioral and cognitive alterations described in PrP-KO animals under these conditions [30, 102–104] could follow impairment of synaptic transmission either at the pre- or post-synaptic level, or both. This same notion may also be valid under neurodegenerative conditions, in which the threat by neurotoxic species adds to the above hypothesized diversion of PrP^C from its physiologic function.

Acknowledgements Authors are grateful to Drs. Domenico Azarnia Tehran and Fiorella Tonello for helpful suggestions on the synaptic vesicle recycling assay, and to Dr. Cesare Montecucco for kindly providing us with the needed serotype of botulinum toxin. This work was supported by the University of Padova (PRAT CPDA158035 to A.B. and CPDA139317 to S.C.). C.P. was supported by a grant to G.A. (CPDR159477/15). Authors also acknowledge the Cassa di Risparmio di Padova e Rovigo (Cariparo) Holding for funding acquisition of the LTQ-Orbitrap XL mass spectrometer.

Compliance with Ethical Standards

All experimental procedures and animal care protocols were approved by the Italian Ministry of Health (authorization no. 743/2017-PR) and by the Ethical Committee for animal care and use of the University of Padova.

Conflict of Interest The authors declare no potential conflict of interest.

References

1. Herms J, Tings T, Gall S, Madlung A, Giese A, Siebert H, Schürmann P, Windl O et al (1999) Evidence of presynaptic location and function of the prion protein. J Neurosci 19:8866–8875
2. Moya KL, Sales N, Hassig R et al (2000) Immunolocalization of the cellular prion protein in normal brain. Microsc Res Tech 50:

58–65. https://doi.org/10.1002/1097-0029(20000701)50:1<58::AID-JEMT9>3.0.CO;2-5
3. Collins MO, Husi H, Yu L, Brandon JM, Anderson CNG, Blackstock WP, Choudhary JS, Grant SGN (2006) Molecular characterization and comparison of the components and multiprotein complexes in the postsynaptic proteome. J Neurochem 97(Suppl 1):16–23. https://doi.org/10.1111/j.1471-4159.2005.03507.x
4. Um JW, Nygaard HB, Heiss JK, Kostylev MA, Stagi M, Vortmeyer A, Wisniewski T, Gunther EC et al (2012) Alzheimer amyloid-beta oligomer bound to postsynaptic prion protein activates Fyn to impair neurons. Nat Neurosci 15:1227–1235. https://doi.org/10.1038/nn.3178
5. DeArmond SJ, Prusiner SB (1995) Etiology and pathogenesis of prion diseases. Am J Pathol 146:785–811
6. Colby DW, Prusiner SB (2011) De novo generation of prion strains. Nat Rev Microbiol 9:771–777. https://doi.org/10.1038/nrmicro2650
7. Bueler H, Aguzzi A, Sailer A et al (1993) Mice devoid of PrP are resistant to scrapie. Cell 73:1339–1347
8. Prusiner SB, Groth D, Serban A, Koehler R, Foster D, Torchia M, Burton D, Yang SL et al (1993) Ablation of the prion protein (PrP) gene in mice prevents scrapie and facilitates production of anti-PrP antibodies. Proc Natl Acad Sci U S A 90:10608–10612
9. Bueler H, Fischer M, Lang Y et al (1992) Normal development and behaviour of mice lacking the neuronal cell-surface PrP protein. Nature 356:577–582. https://doi.org/10.1038/356577a0
10. Manson JC, Clarke A, Hooper ML et al (1994) 129/Ola mice carrying a null mutation in PrP that abolishes mRNA production are developmentally normal. Mol Neurobiol 8:121–127
11. Castle AR, Gill AC (2017) Physiological functions of the cellular prion protein. Front Mol Biosci 4:19. https://doi.org/10.3389/fmolb.2017.00019
12. Linden R (2017) The biological function of the prion protein: a cell surface scaffold of signaling modules. Front Mol Neurosci 10:77
13. Peggion C, Bertoli A, Sorgato MC (2017) Almost a century of prion protein(s): from pathology to physiology, and back to pathology. Biochem Biophys Res Commun 483:1148–1155. https://doi.org/10.1016/j.bbrc.2016.07.118
14. Wulf M-A, Senatore A, Aguzzi A (2017) The biological function of the cellular prion protein: an update. BMC Biol 15:34. https://doi.org/10.1186/s12915-017-0375-5
15. Watts JC, Bourkas MEC, Arshad H (2018) The function of the cellular prion protein in health and disease. Acta Neuropathol 135:159–178. https://doi.org/10.1007/s00401-017-1790-y
16. Zahn R, Liu A, Luhrs T, Riek R, von Schroetter C, Lopez Garcia F, Billeter M, Calzolai L et al (2000) NMR solution structure of the human prion protein. Proc Natl Acad Sci U S A 97:145–150
17. van der Lee R, Lang B, Kruse K, Gsponer J, Sánchez de Groot N, Huynen MA, Matouschek A, Fuxreiter M et al (2014) Intrinsically disordered segments affect protein half-life in the cell and during evolution. Cell Rep 8:1832–1844. https://doi.org/10.1016/j.celrep.2014.07.055
18. Tompa P, Schad E, Tantos A, Kalmar L (2015) Intrinsically disordered proteins: emerging interaction specialists. Curr Opin Struct Biol 35:49–59. https://doi.org/10.1016/j.sbi.2015.08.009
19. Lauren J, Gimbel DA, Nygaard HB et al (2009) Cellular prion protein mediates impairment of synaptic plasticity by amyloid-beta oligomers. Nature 457:1128–1132. https://doi.org/10.1038/nature07761
20. Resenberger UK, Harmeier A, Woerner AC, Goodman JL, Müller V, Krishnan R, Vabulas RM, Kretzschmar HA et al (2011) The cellular prion protein mediates neurotoxic signalling of beta-sheet-rich conformers independent of prion replication. EMBO J 30:2057–2070. https://doi.org/10.1038/emboj.2011.86
21. Ferreira DG, Temido-Ferreira M, Miranda HV, Batalha VL, Coelho JE, Szegö ÉM, Marques-Morgado I, Vaz SH et al (2017) Alpha-synuclein interacts with PrP(C) to induce cognitive impairment through mGluR5 and NMDAR2B. Nat Neurosci 20:1569–1579. https://doi.org/10.1038/nn.4648
22. Aulic S, Masperone L, Narkiewicz J et al (2017) Alpha-synuclein amyloids hijack prion protein to gain cell entry, facilitate cell-to-cell spreading and block prion replication. Sci Rep 7:10050. https://doi.org/10.1038/s41598-017-10236-x
23. Urrea L, Segura-Feliu M, Masuda-Suzukake M, Hervera A, Pedraz L, García Aznar JM, Vila M, Samitier J et al (2017) Involvement of cellular prion protein in alpha-synuclein transport in neurons. Mol Neurobiol 55:1847–1860. https://doi.org/10.1007/s12035-017-0451-4
24. Collinge J, Whittington MA, Sidle KC et al (1994) Prion protein is necessary for normal synaptic function. Nature 370:295–297. https://doi.org/10.1038/370295a0
25. Manson JC, Hope J, Clarke AR, Johnston A, Black C, MacLeod N (1995) PrP gene dosage and long term potentiation. Neurodegeneration 4:113–114
26. Carleton A, Tremblay P, Vincent JD, Lledo PM (2001) Dose-dependent, prion protein (PrP)-mediated facilitation of excitatory synaptic transmission in the mouse hippocampus. Pflugers Arch 442:223–229
27. Re L, Rossini F, Re F et al (2006) Prion protein potentiates acetylcholine release at the neuromuscular junction. Pharmacol Res 53:62–68. https://doi.org/10.1016/j.phrs.2005.09.002
28. Prestori F, Rossi P, Bearzatto B, Laine J, Necchi D, Diwakar S, Schiffmann SN, Axelrad H et al (2008) Altered neuron excitability and synaptic plasticity in the cerebellar granular layer of juvenile prion protein knock-out mice with impaired motor control. J Neurosci 28:7091–7103. https://doi.org/10.1523/JNEUROSCI.0409-08.2008
29. Robinson SW, Nugent ML, Dinsdale D, Steinert JR (2014) Prion protein facilitates synaptic vesicle release by enhancing release probability. Hum Mol Genet 23:4581–4596. https://doi.org/10.1093/hmg/ddu171
30. Schmitz M, Greis C, Ottis P, Silva CJ, Schulz-Schaeffer WJ, Wrede A, Koppe K, Onisko B et al (2014) Loss of prion protein leads to age-dependent behavioral abnormalities and changes in cytoskeletal protein expression. Mol Neurobiol 50:923–936. https://doi.org/10.1007/s12035-014-8655-3
31. Mallucci GR, Ratté S, Asante EA, Linehan J, Gowland I, Jefferys JGR, Collinge J (2002) Post-natal knockout of prion protein alters hippocampal CA1 properties, but does not result in neurodegeneration. EMBO J 21:202–210. https://doi.org/10.1093/emboj/21.3.202
32. Lazzari C, Peggion C, Stella R, Massimino ML, Lim D, Bertoli A, Sorgato MC (2011) Cellular prion protein is implicated in the regulation of local Ca2+ movements in cerebellar granule neurons. J Neurochem 116:881–890. https://doi.org/10.1111/j.1471-4159.2010.07015.x
33. Azarnia Tehran D, Zanetti G, Leka O, Lista F, Fillo S, Binz T, Shone CC, Rossetto O et al (2015) A novel inhibitor prevents the peripheral neuroparalysis of botulinum neurotoxins. Sci Rep 5:17513. https://doi.org/10.1038/srep17513
34. Boersema PJ, Raijmakers R, Lemeer S, Mohammed S, Heck AJR (2009) Multiplex peptide stable isotope dimethyl labeling for quantitative proteomics. Nat Protoc 4:484–494. https://doi.org/10.1038/nprot.2009.21
35. Wisniewski JR, Zougman A, Nagaraj N, Mann M (2009) Universal sample preparation method for proteome analysis. Nat Methods 6:359–362. https://doi.org/10.1038/nmeth.1322
36. MacLean B, Tomazela DM, Shulman N, Chambers M, Finney GL, Frewen B, Kern R, Tabb DL et al (2010) Skyline: an open source document editor for creating and analyzing targeted

proteomics experiments. Bioinformatics 26:966–968. https://doi.org/10.1093/bioinformatics/btq054
37. Welinder C, Ekblad L (2011) Coomassie staining as loading control in western blot analysis. J Proteome Res 10:1416–1419. https://doi.org/10.1021/pr1011476
38. Wang J, Duncan D, Shi Z, Zhang B (2013) WEB-based GEne SeT AnaLysis toolkit (WebGestalt): update 2013. Nucleic Acids Res 41:W77–W83
39. Kwon AT, Arenillas DJ, Worsley Hunt R, Wasserman WW (2012) oPOSSUM-3: advanced analysis of regulatory motif over-representation across genes or ChIP-Seq datasets. G3 (Bethesda) 2:987–1002. https://doi.org/10.1534/g3.112.003202
40. Sandelin A, Alkema W, Engstrom P et al (2004) JASPAR: an open-access database for eukaryotic transcription factor binding profiles. Nucleic Acids Res 32:D91–D94. https://doi.org/10.1093/nar/gkh012
41. Schiavo G, Benfenati F, Poulain B et al (1992) Tetanus and botulinum-B neurotoxins block neurotransmitter release by proteolytic cleavage of synaptobrevin. Nature 359:832–835. https://doi.org/10.1038/359832a0
42. Maximov A, Sudhof TC (2005) Autonomous function of synaptotagmin 1 in triggering synchronous release independent of asynchronous release. Neuron 48:547–554. https://doi.org/10.1016/j.neuron.2005.09.006
43. Stella R, Cifani P, Peggion C, Hansson K, Lazzari C, Bendz M, Levander F, Sorgato MC et al (2012) Relative quantification of membrane proteins in wild-type and prion protein (PrP)-knockout cerebellar granule neurons. J Proteome Res 11:523–536
44. Yang X-Z, Li X-X, Zhang Y-J, Rodriguez-Rodriguez L, Xiang MQ, Wang HY, Zheng XFS (2016) Rab1 in cell signaling, cancer and other diseases. Oncogene 35:5699–5704. https://doi.org/10.1038/onc.2016.81
45. Kaeser PS, Deng L, Wang Y, Dulubova I, Liu X, Rizo J, Südhof TC (2011) RIM proteins tether Ca2+ channels to presynaptic active zones via a direct PDZ-domain interaction. Cell 144:282–295. https://doi.org/10.1016/j.cell.2010.12.029
46. Guerra F, Bucci C (2016) Multiple roles of the small GTPase Rab7. Cells 5:3. https://doi.org/10.3390/cells5030034
47. Sönnichsen B, De Renzis S, Nielsen E et al (2000) Distinct membrane domains on endosomes in the recycling pathway visualized by multicolor imaging of Rab4, Rab5, and Rab11. J Cell Biol 149:901–914
48. Gerber SH, Rah J-C, Min S-W, Liu X, de Wit H, Dulubova I, Meyer AC, Rizo J et al (2008) Conformational switch of syntaxin-1 controls synaptic vesicle fusion. Science 321:1507–1510. https://doi.org/10.1126/science.1163174
49. Belizaire R, Komanduri C, Wooten K, Chen M, Thaller C, Janz R (2004) Characterization of synaptogyrin 3 as a new synaptic vesicle protein. J Comp Neurol 470:266–281. https://doi.org/10.1002/cne.20008
50. Burré J, Sharma M, Tsetsenis T et al (2010) α-Synuclein promotes SNARE-complex assembly in vivo and in vitro. Science 329:1663–1667
51. Mosevitsky MI (2005) Nerve ending "signal" proteins GAP-43, MARCKS, and BASP1. Int Rev Cytol 245:245–325. https://doi.org/10.1016/S0074-7696(05)45007-X
52. Mehrabian M, Brethour D, Williams D, Wang H, Arnould H, Schneider B, Schmitt-Ulms G (2016) Prion protein deficiency causes diverse proteome shifts in cell models that escape detection in brain tissue. PLoS One 11:e0142287. https://doi.org/10.1371/journal.pone.0156779
53. Picotti P, Aebersold R (2012) Selected reaction monitoring-based proteomics: workflows, potential, pitfalls and future directions. Nat Methods 9:555–566. https://doi.org/10.1038/nmeth.2015
54. Mallick P, Schirle M, Chen SS, Flory MR, Lee H, Martin D, Ranish J, Raught B et al (2007) Computational prediction of proteotypic peptides for quantitative proteomics. Nat Biotechnol 25:125–131. https://doi.org/10.1038/nbt1275
55. Pradines E, Loubet D, Schneider B, Launay JM, Kellermann O, Mouillet-Richard S (2008) CREB-dependent gene regulation by prion protein: impact on MMP-9 and β-dystroglycan. Cell Signal 20:2050–2058. https://doi.org/10.1016/j.cellsig.2008.07.016
56. Choi J-K, Jeon Y-C, Lee D-W, Oh JM, Lee HP, Jeong BH, Carp RI, Koh YH et al (2010) A Drosophila model of GSS syndrome suggests defects in active zones are responsible for pathogenesis of GSS syndrome. Hum Mol Genet 19:4474–4489. https://doi.org/10.1093/hmg/ddq379
57. Wandinger-Ness A, Zerial M (2014) Rab proteins and the compartmentalization of the endosomal system. Cold Spring Harb Perspect Biol 6:a022616. https://doi.org/10.1101/cshperspect.a022616
58. Fischer von Mollard G, Mignery GA, Baumert M, Perin MS, Hanson TJ, Burger PM, Jahn R, Sudhof TC (1990) rab3 is a small GTP-binding protein exclusively localized to synaptic vesicles. Proc Natl Acad Sci U S A 87:1988–1992. https://doi.org/10.1073/pnas.87.5.1988
59. Castillo PE, Janz R, Sudhof TC et al (1997) Rab3A is essential for mossy fibre long-term potentiation in the hippocampus. Nature 388:590–593. https://doi.org/10.1038/41574
60. Graf ER, Daniels RW, Burgess RW, Schwarz TL, DiAntonio A (2009) Rab3 dynamically controls protein composition at active zones. Neuron 64:663–677
61. Deinhardt K, Salinas S, Verastegui C, Watson R, Worth D, Hanrahan S, Bucci C, Schiavo G (2006) Rab5 and Rab7 control endocytic sorting along the axonal retrograde transport pathway. Neuron 52:293–305. https://doi.org/10.1016/j.neuron.2006.08.018
62. McInnes J, Wierda K, Snellinx A, Bounti L, Wang YC, Stancu IC, Apóstolo N, Gevaert K et al (2018) Synaptogyrin-3 mediates presynaptic dysfunction induced by tau. Neuron 97:823–835. https://doi.org/10.1016/j.neuron.2018.01.022
63. Mishima T, Fujiwara T, Sanada M, Kofuji T, Kanai-Azuma M, Akagawa K (2014) Syntaxin 1B, but not syntaxin 1A, is necessary for the regulation of synaptic vesicle exocytosis and of the readily releasable pool at central synapses. PLoS One 9:e90004. https://doi.org/10.1371/journal.pone.0090004
64. Sudhof TC, Rothman JE (2009) Membrane fusion: grappling with SNARE and SM proteins. Science 323:474–477. https://doi.org/10.1126/science.1161748
65. Zafar S, Von Ahsen N, Oellerich M et al (2011) Proteomics approach to identify the interacting partners of cellular prion protein and characterization of rab7a interaction in neuronal cells. J Proteome Res 10:3123–3135. https://doi.org/10.1021/pr2001989
66. Fassio A, Fadda M, Benfenati F (2016) Molecular machines determining the fate of endocytosed synaptic vesicles in nerve terminals. Front Synaptic Neurosci 8:10. https://doi.org/10.3389/fnsyn.2016.00010
67. Black SAG, Stys PK, Zamponi GW, Tsutsui S (2014) Cellular prion protein and NMDA receptor modulation: protecting against excitotoxicity. Front Cell Dev Biol 2:45. https://doi.org/10.3389/fcell.2014.00045
68. Bertoli A, Sorgato MC (2018) Neuronal pathophysiology featuring PrP(C) and its control over Ca(2+) metabolism. Prion 12:28–33. https://doi.org/10.1080/19336896.2017.1412912
69. De Mario A, Castellani A, Peggion C et al (2015) The prion protein constitutively controls neuronal store-operated Ca(2+) entry through Fyn kinase. Front Cell Neurosci 9:416. https://doi.org/10.3389/fncel.2015.00416
70. Senatore A, Colleoni S, Verderio C, Restelli E, Morini R, Condliffe SB, Bertani I, Mantovani S et al (2012) Mutant PrP suppresses glutamatergic neurotransmission in cerebellar granule neurons by impairing membrane delivery of VGCC alpha(2)delta-

1 subunit. Neuron 74:300–313. https://doi.org/10.1016/j.neuron.2012.02.027
71. Ferrer I, Puig B, Blanco R, Martì E (2000) Prion protein deposition and abnormal synaptic protein expression in the cerebellum in Creutzfeldt–Jakob disease. Neuroscience 97:715–726. https://doi.org/10.1016/S0306-4522(00)00045-2
72. Gawinecka J, Cardone F, Asif AR, de Pascalis A, Wemheuer WM, Schulz-Schaeffer WJ, Pocchiari M, Zerr I (2012) Sporadic Creutzfeldt–Jakob disease subtype-specific alterations of the brain proteome: impact on Rab3a recycling. Proteomics 12:3610–3620
73. Shim SY, Karri S, Law S, Schatzl HM, Gilch S (2016) Prion infection impairs lysosomal degradation capacity by interfering with rab7 membrane attachment in neuronal cells. Sci Rep 6:21658. https://doi.org/10.1038/srep21658
74. Ermolayev V, Cathomen T, Merk J, Friedrich M, Härtig W, Harms GS, Klein MA, Flechsig E (2009) Impaired axonal transport in motor neurons correlates with clinical prion disease. PLoS Pathog 5:e1000558. https://doi.org/10.1371/journal.ppat.1000558
75. Massignan T, Biasini E, Lauranzano E, Veglianese P, Pignataro M, Fioriti L, Harris DA, Salmona M et al (2010) Mutant prion protein expression is associated with an alteration of the Rab GDP dissociation inhibitor alpha (GDI)/Rab11 pathway. Mol Cell Proteomics 9:611–622. https://doi.org/10.1074/mcp.M900271-MCP200
76. Schubert J, Siekierska A, Langlois M et al (2014) Mutations in STX1B, encoding a presynaptic protein, cause fever-associated epilepsy syndromes. Nat Genet 46:1327–1332. https://doi.org/10.1038/ng.3130
77. Wang J-Y, Gong M-Y, Ye Y-L, Ye JM, Lin GL, Zhuang QQ, Zhang X, Zhu JH (2015) The RIT2 and STX1B polymorphisms are associated with Parkinson's disease. Parkinsonism Relat Disord 21:300–302. https://doi.org/10.1016/j.parkreldis.2014.12.006
78. Nixon RR (2005) Prion-associated increases in Src-family kinases. J Biol Chem 280:2455–2462. https://doi.org/10.1074/jbc.M410883200
79. Chiti Z, Knutsen OM, Betmouni S, Greene JRT (2006) An integrated, temporal study of the behavioural, electrophysiological and neuropathological consequences of murine prion disease. Neurobiol Dis 22:363–373. https://doi.org/10.1016/j.nbd.2005.12.002
80. Sorgato MC, Bertoli A (2009) From cell protection to death: May Ca2+ signals explain the chameleonic attributes of the mammalian prion protein? Biochem Biophys Res Commun 379:171–174. https://doi.org/10.1016/j.bbrc.2008.12.026
81. You H, Tsutsui S, Hameed S, Kannanayakal TJ, Chen L, Xia P, Engbers JDT, Lipton SA et al (2012) A Aβ neurotoxicity depends on interactions between copper ions, prion protein, and N-methyl-D-aspartate receptors. Proc Natl Acad Sci 109:1737–1742. https://doi.org/10.1073/pnas.1110789109
82. Hu N-W, Nicoll AJ, Zhang D, Mably AJ, O'Malley T, Purro SA, Terry C, Collinge J et al (2014) mGlu5 receptors and cellular prion protein mediate amyloid-beta-facilitated synaptic long-term depression in vivo. Nat Commun 5:3374. https://doi.org/10.1038/ncomms4374
83. Mouillet-Richard S (2000) Signal transduction through prion protein. Science 289:1925–1928
84. Chen S, Mangé A, Dong L, Lehmann S, Schachner M (2003) Prion protein as trans-interacting partner for neurons is involved in neurite outgrowth and neuronal survival. Mol Cell Neurosci 22:227–233. https://doi.org/10.1016/S1044-7431(02)00014-3
85. Khosravani H, Zhang Y, Tsutsui S, Hameed S, Altier C, Hamid J, Chen L, Villemaire M et al (2008) Prion protein attenuates excitotoxicity by inhibiting NMDA receptors. J Cell Biol 181:551–555. https://doi.org/10.1083/jcb.200711002
86. De Mario A, Peggion C, Massimino ML et al (2017) The prion protein regulates glutamate-mediated Ca(2+) entry and mitochondrial Ca(2+) accumulation in neurons. J Cell Sci 130:2736–2746. https://doi.org/10.1242/jcs.196972
87. Bagetta V, Ghiglieri V, Sgobio C, Calabresi P, Picconi B (2010) Synaptic dysfunction in Parkinson's disease. Biochem Soc Trans 38:493–497. https://doi.org/10.1042/BST0380493
88. Milnerwood AJ, Raymond LA (2010) Early synaptic pathophysiology in neurodegeneration: insights from Huntington's disease. Trends Neurosci 33:513–523. https://doi.org/10.1016/j.tins.2010.08.002
89. Selkoe DJ, Hardy J (2016) The amyloid hypothesis of Alzheimer's disease at 25 years. EMBO Mol Med 8:595–608. https://doi.org/10.15252/emmm.201606210
90. Crecelius AC, Helmstetter D, Strangmann J, Mitteregger G, Fröhlich T, Arnold GJ, Kretzschmar HA (2008) The brain proteome profile is highly conserved between Prnp−/− and Prnp+/+ mice. Neuroreport 19:1027–1031. https://doi.org/10.1097/WNR.0b013e3283046157
91. Chadi S, Young R, Le Guillou S et al (2010) Brain transcriptional stability upon prion protein-encoding gene invalidation in zygotic or adult mouse. BMC Genomics 11:448. https://doi.org/10.1186/1471-2164-11-448
92. Satoh J, Kuroda Y, Katamine S (2000) Gene expression profile in prion protein-deficient fibroblasts in culture. Am J Pathol 157:59–68
93. Ramljak S, Asif AR, Armstrong VW, Wrede A, Groschup MH, Buschmann A, Schulz-Schaeffer W, Bodemer W et al (2008) Physiological role of the cellular prion protein (PrPc): protein profiling study in two cell culture systems research articles. J Proteome Res 7:2681–2695. https://doi.org/10.1021/pr70071872681-2695
94. Weiss E, Ramljak S, Asif AR, Ciesielczyk B, Schmitz M, Gawinecka J, Schulz-Schaeffer W, Behrens C et al (2010) Cellular prion protein overexpression disturbs cellular homeostasis in SH-SY5Y neuroblastoma cells but does not alter p53 expression: a proteomic study. Neuroscience 169:1640–1650. https://doi.org/10.1016/j.neuroscience.2010.06.013
95. Johannessen M, Delghandi MP, Moens U (2004) What turns CREB on? Cell Signal 16:1211–1227. https://doi.org/10.1016/j.cellsig.2004.05.001
96. Benito E, Barco A (2010) CREB's control of intrinsic and synaptic plasticity: implications for CREB-dependent memory models. Trends Neurosci 33:230–240. https://doi.org/10.1016/j.tins.2010.02.001
97. Spudich A, Frigg R, Kilic E, Kilic Ü, Oesch B, Raeber A, Bassetti CL, Hermann DM (2005) Aggravation of ischemic brain injury by prion protein deficiency: role of ERK-1/-2 and STAT-1. Neurobiol Dis 20:442–449. https://doi.org/10.1016/j.nbd.2005.04.002
98. Weise J, Sandau R, Schwarting S, Crome O, Wrede A, Schulz-Schaeffer W, Zerr I, Bahr M (2006) Deletion of cellular prion protein results in reduced Akt activation, enhanced postischemic caspase-3 activation, and exacerbation of ischemic brain injury. Stroke 37:1296–1300. https://doi.org/10.1161/01.STR.0000217262.03192.d4
99. Gadotti VM, Bonfield SP, Zamponi GW (2012) Depressive-like behaviour of mice lacking cellular prion protein. Behav Brain Res 227:319–323. https://doi.org/10.1016/j.bbr.2011.03.012
100. Carulla P, Llorens F, Matamoros-Angles A, Aguilar-Calvo P, Espinosa JC, Gavín R, Ferrer I, Legname G et al (2015) Involvement of PrP(C) in kainate-induced excitotoxicity in several mouse strains. Sci Rep 5:11971. https://doi.org/10.1038/srep11971
101. Doeppner TR, Kaltwasser B, Schlechter J, Jaschke J, Kilic E, Bähr M, Hermann DM, Weise J (2015) Cellular prion protein promotes post-ischemic neuronal survival, angioneurogenesis and enhances neural progenitor cell homing via proteasome inhibition. Cell Death Dis 6:e2024. https://doi.org/10.1038/cddis.2015.365

102. Sanchez-Alavez M, Conti B, Moroncini G, Criado JR (2007) Contributions of neuronal prion protein on sleep recovery and stress response following sleep deprivation. Brain Res 1158:71–80. https://doi.org/10.1016/j.brainres.2007.05.010
103. Nazor KE, Seward T, Telling GC (2007) Motor behavioral and neuropathological deficits in mice deficient for normal prion protein expression. Biochim Biophys Acta 1772:645–653. https://doi.org/10.1016/j.bbadis.2007.04.004
104. Massimino ML, Redaelli M, Bertoli A, Sorgato MC, Mucignat-Caretta C (2013) Altered behavioral aspects of aged mice lacking the cellular prion protein. Physiol Behav 119:86–91. https://doi.org/10.1016/j.physbeh.2013.06.006